Journal of Sound and Vibration (1999) **225**(5), 887–913
Article No. jsvi.1999.2252, available online at http://www.idealibrary.com on IDEAL®

WAVELET ANALYSIS FOR HOPF BIFURCATIONS WITH AEROELASTIC APPLICATIONS

F. MASTRODDI AND A. BETTOLI

Dipartimento Aerospaziale, Università degli Studi di Roma "La Sapienza"
via Eudossiana 16, 00184 *Rome, Italy*

(*Received* 13 *July* 1998, *and in final form* 15 *February* 1999)

A wavelet analysis on the output signal of a non-linear system in the neighbourhood of a Hopf bifurcation (i.e., a limit-cycle oscillation) has been performed to point out the linear and non-linear signatures of the system. Indeed, this kind of non-linear behaviour is characterized not only by a simple harmonic oscillation in developed steady state condition, but also by an initial transitory phase with a complex time evolution of the spectral signal content. Both these issues could be described in an analytical way via a singular perturbation analysis but they could be also directly analyzed by a signal-processing tool via wavelet analysis (Continuous Wavelet Transform, CWT): this is obtained by using the wavelet capability in describing efficiently the time evolution of the spectrum of the signal (i.e., a non-linear "signature" of a Hopf bifurcation). Furthermore, the analytical results given by the singular perturbation analysis for the same class of non-linear problems, have allowed one to interpret correctly the results obtained by the wavelet analysis. In this paper this theoretical link between the wavelet analysis and the output signal of a dynamical system (recently achieved for linear mechanical damped systems) has been extended to non-linear systems in the neighbourhood of a Hopf bifurcation. This kind of analysis is of natural interest in aeroelastic applications where an efficient (and noise insensitive) analysis of the output signal recorded during the flight tests performed in the neighbourhood of the critical condition (flutter) may be desirable together with the capability to record the non-linear system signature. The time-scale decompositions (CWT) have given the opportunity to analyze pre- and post-critical transient behaviour of a non-linear aeroelastic system and, thus, upon considering the analytical tool given by the singular perturbation analysis, to identify its linear and non-linear features. Applications include either two non-linear coupled oscillators or a typical section in a supersonic flow.

1. INTRODUCTION

Experimental tests are an essential issue for the identification of dynamical systems. Tests are also necessary *a posteriori* to tune the numerical model to the real system and to "update" the numerical model as well. Furthermore, in the field of aeroelasticity, flight tests are also essential because they can give an estimate of systems stability margins [1].

0022-460X/99/350887 + 27 $30.00/0

On the other hand, one has also to consider that the design of experimental flight tests and their final results are both highly affected by the methods available for processing and analyzing the data recorded during the test. Indeed, the identification methods based on wavelet transforms have shown several advantages in aeroelastic analysis with respect to the standard ones, above all for the "de-noising" effects included in the method: in references [1, 2] an overview of flight-test data analysis using wavelets for aeroelastic system identification and de-noising was shown; the wavelet tools have been also used for the modal parameters identification of linear structural–dynamical systems in references [3–5]; moreover, in reference to the class of aeroelastic problems, in references [6, 7] the evaluation of the stability margin with respect to a given parameter (e.g., the flight speed) based on measured data was presented as a relevant issue.

Nevertheless, for both system identification and stability-margin identification, the transient nature of the inflight aeroelastic dynamics (intermittency, modulation, non-periodicity, non-stationarity, time-variance and non-linearity in the data) seems to show the standard Fourier analysis to be inadequate. Because of these reasons, time-scale analyses have recently been developed in this field, these tools having more suitable features for the mentioned problems than the classical methods of signal processing analysis. Specifically, wavelets are waveforms that, once correlated to the signal, allow one to localize in time and frequency the signal energetic content with arbitrary high resolution in time at high frequencies and arbitrary high-frequency resolution at low frequencies: in this way, one can identify the features of the signal localized or spread both in time and frequency. Assuming that the transient of the energetic content of the output signal is generally a very relevant signature of systems (e.g., consider the impulse response for linear systems), one may realize the wavelet capabilities for the identification of the main features of linear and non-linear systems and, in particular, their stability margins.

In this paper the description offered by the wavelet analysis for system responses (used for the identification of linear mechanical systems in reference [4] and applied in reference [7] for the stability-margin estimate of non-linear system) has been studied interpreting the obtained results via a singular perturbation analysis [8]. To achieve this goal (see also reference [9]), a wavelet analysis of the response—to initial conditions—of non-linear systems in the neighbourhood of a Hopf bifurcation (i.e., limit cycle behaviour) will be examined with the support of the analytical predictions given by a singular perturbation method: one-parameter autonomous dynamical systems, with algebraic non-linearities and admitting trivial steady state solution, will be considered. The parameter will be denoted by μ, and the analyses will be performed in the neighbourhood of its critical value μ_0, for which the linear analysis predicts the transition from stable to unstable behaviour. Then, it is assumed that for $\mu < \mu_0$, the steady-state solution $x = 0$ is linearly stable, in the sense that all the eigenvalues of the perturbation matrix around $x = 0$ have a negative real part; moreover, it is assumed that, at $\mu = \mu_0$, the system experiences a Hopf bifurcation in the sense that one (and only one) pair of complex conjugate eigenvalues crosses the imaginary axis [10]. As emphasized in most of the papers in the field of non-linear aeroelasticity (see reference [11] for a recent and rich review

on the subject), this mathematical description is physically performed by most of the aeroelastic systems in the neighbourhood of their critical stability margin: in this case, μ is typically the flight speed U_∞, the instability connected with the Hopf bifurcation is flutter, and then μ_0 is referred to as the flutter speed ($U_{\infty F}$). The analytical solution for the transient and steady state behaviour will be expressed by using an asymptotic-expansion obtained in reference [12] through a singular perturbation method.

In the first part of the paper the general analytical solutions available by the singular perturbation analysis are analyzed; next, it is shown how this approach allows one to predict the most relevant non-linear features of the non-linear systems response. In the same section an overview of the continuous wavelet transforms (CWT) is given and a theoretical connection between the analytical predictions (by the singular perturbation analysis) and the results obtained by a CWT analysis of the time response is established. In the second part, two applications will be examined: the first concerns a simple MDOF non-linear dynamical system, while the second concerns an airfoil in a supersonic flow.

2. THEORETICAL BASIS

Consider a general non-linear system represented in state space by

$$\dot{\mathbf{z}} = \mathbf{A}(\mu)\mathbf{z} + \mathbf{f}(\mathbf{z}, \mu), \tag{1}$$

where $\mathbf{z} \in \mathbf{R}^{N_s}$ (N_s is the state-space dimension) is the state-space vector, $\mathbf{A}$ represents the linear part of the system, $\mathbf{f}$ the non-linear part (without loss of generality, only algebraic non-linearities are considered), and μ is a parameter.

Suppose that if $\mu < \mu_0$, the trivial solution of the linear part of the system is stable (all of the eigenvalues of $\mathbf{A}$ have negative real part), while if $\mu > \mu_0$ the linear part of the system is unstable (there is at least one real eigenvalue or a complex conjugate pair of eigenvalues with positive real part).

Considering, for the sake of simplicity, only cubic non-linearities, one has

$$\mathbf{f}(\mathbf{z}, \mu) = \left\{ \sum_{p,q,r=1}^{N_s} c_{npqr}(\mu)\, z_p z_q Z_r \right\}. \tag{2}$$

where $c_{npqr}(\mu)$ is a $N_s \times N_s \times N_s \times N_s$ non-linear-coefficient matrix. In the next section, the general solution for the above system in the neighbourhood of a Hopf bifurcation will be analytically obtained (see references [12, 13] for details on the singular perturbation method used in this paper); next, the basic concepts of the CWT analysis will be presented in section 2.2 and, finally, the theoretical relationship between these two different point of views will be shown in section 2.3.

2.1. HOPF BIFURCATION VIA SINGULAR PERTURBATION ANALYSIS

The system given by equation (1) has been considered in the neighbourhood of a limit cycle solution (i.e., for $\mu \simeq \mu_0$). Calling $\varepsilon = |\mu - \mu_0|$ a small-perturbation parameter, one has

$$\mu = \mu_0 \pm \varepsilon, \tag{3}$$

where the plus (minus) holds for post-critical (pre-critical) response. It is supposed that for $\mu = \mu_0$ a couple (and only one) of eigenvalues of the matrix $\mathbf{A}$ have real parts equal to zero (say $\lambda_{1,2} = \pm \mathrm{j}\omega_0$) while the remaining eigenvalues are still stable. Calling $\mathbf{A}_0 = \mathbf{A}(\mu_0)$, $\mathbf{A}_1 = \partial\mathbf{A}/\partial\mu|_{\mu=\mu_0}$, one has

$$\mathbf{A}(\mu) = \mathbf{A}_0 \pm \varepsilon\mathbf{A}_1 + \mathcal{O}(\varepsilon^2), \tag{4}$$

while $c_{npqr}(\mu) = c_{npqr}(\mu_0) + \mathcal{O}(\varepsilon)$. Upon considering

$$\mathbf{z} = \sqrt{\varepsilon}\,\mathbf{U}\mathbf{x}, \tag{5}$$

where $\mathbf{U}$ is the eigenvector matrix of $\mathbf{A}_0$ (it is assumed that in the first two columns of $\mathbf{U}$ there are the eigenvectors $\mathbf{u}^{(1)}, \mathbf{u}^{(2)}$ corresponding to the critical eigenvalues $\lambda_{1,2}$), equation (1) becomes

$$\dot{\mathbf{x}} = \mathbf{\Lambda}_0\mathbf{x} + \varepsilon\left\{ \pm \sum_{s=1}^{N_s} \alpha_{js} x_s + \sum_{p,q,r=1}^{N_s} \gamma_{jpqr} x_p x_q x_r \right\}, \tag{6}$$

where $\mathbf{\Lambda}_0$ is the diagonal matrix containing the $\mathbf{A}_0$ eigenvalues and

$$\alpha_{js} := \sum_{l,m=1}^{N_s} U_{jl}^{-1} A_{1_{lm}} U_{ms}, \qquad \gamma_{jpqr} := \sum_{s,t,u,v=1}^{N_s} U_{js}^{-1} c_{stuv} U_{tp} U_{uq} U_{vr}. \tag{7, 8}$$

Applying a "zero divisors" procedure, i.e. searching a transformed problem through the "near-identity transformation" (see e.g., reference [8] for the theoretical details and references [12, 13] for applications of the method in aeroelasticity),

$$\mathbf{x} = \mathbf{y} + \mathbf{h}(\mathbf{y}, \varepsilon), \tag{9}$$

given by the vector $\mathbf{h}(\mathbf{y}, \varepsilon)$, one obtains

$$\dot{\mathbf{y}} = \mathbf{\Lambda}_0\mathbf{y} + \varepsilon\left\{ \pm \sum_{s=1}^{N_s} \alpha_{js}^{\mathrm{ess}} y_s + \sum_{p,q,r=1}^{N_s} \gamma_{jpqr}^{\mathrm{ess}} y_p y_q y_r \right\}, \tag{10}$$

where

$$\alpha_{js}^{\mathrm{ess}} = \alpha_{js} \quad \text{if } \lambda_s - \lambda_j = 0, \qquad \alpha_{\mathrm{js}}^{\mathrm{ess}} = 0 \quad \text{if } \lambda_s - \lambda_j \neq 0, \tag{11}$$

and

$$\begin{aligned} \gamma^{\text{ess}}_{jpqr} &= \gamma_{jpqr} \quad \text{if } \lambda_p + \lambda_q + \lambda_r - \lambda_j = 0, \\ \gamma^{\text{ess}}_{jpqr} &= 0 \quad \text{if } \lambda_p + \lambda_q + \lambda_r - \lambda_j \neq 0. \end{aligned} \tag{12}$$

Note that the first two scalar equations given by equation (10) are uncoupled with the remainders. Upon using the polar-co-ordinate change

$$y_1 = A_1 \, \mathrm{e}^{\mathrm{j}\varphi_1}, \qquad y_2 = A_1 \, \mathrm{e}^{-\mathrm{j}\varphi_1}, \tag{13}$$

the amplitude A_1 and phase φ_1 of the critical mode (corresponding to the eigenvalues λ_1, λ_2) are given by (see references [15, 12, 10])

$$A_1 = \left[\frac{-\beta_R^{(1)}/\gamma_R^{(1)}}{1 + k \, \mathrm{e}^{2\beta_R^{(1)} t}} \right]^{1/2} \tag{14}$$

$$\varphi_1 = t(-\beta_I^{(1)} + \gamma_I^{(1)} \beta_R^{(1)} / \gamma_R^{(1)}) + (\gamma_I^{(1)}/\gamma_R^{(1)}) \ln(A_1) + \varphi_1^0, \tag{15}$$

where k, φ_1^0 depend on the initial conditions and

$$\beta^{(1)} := \beta_R^{(1)} + \mathrm{j}\beta_I^{(1)} = -\mathrm{j}\omega_0 \mp \varepsilon \alpha_{11} = -\mathrm{j}\omega_0 \mp \varepsilon \mathbf{v}^{(1)\mathrm{T}} \mathbf{A}_1 \mathbf{u}^{(1)}, \tag{16}$$

$$\begin{aligned} \gamma^{(1)} &:= \gamma_{\mathrm{R}}^{(1)} + \mathrm{j}\gamma_{\mathrm{I}}^{(1)} = -\varepsilon(\gamma_{1211} + \gamma_{1121} + \gamma_{1112}), \\ &= -\varepsilon \mathbf{v}^{(1)^{\mathrm{T}}} \left\{ \sum_{p,q,r=1}^{N_s} c_{jpqr} (u_p^{(1)*} u_q^{(1)} u_r^{(1)} + u_p^{(1)} u_q^{(1)*} u_r^{(1)} + u_p^{(1)} u_q^{(1)} u_r^{(1)*}) \right\}. \end{aligned} \tag{17}$$

Considering the other $N_s - 2$ equations corresponding to complex eigenvalues with negative real part,[†] one obtains equations that can be solved sequentially and then, by using equations (14) and (15), one has

$$A_n = A_n^0 (A_1/A_1^0)^{\gamma_R^{(n)}/\gamma_R^{(1)}} \, \mathrm{e}^{t(-\beta_R^{(n)} + \beta_R^{(1)} \gamma_R^{(n)}/\gamma_R^{(1)})}, \tag{18}$$

$$\varphi_n = t(-\beta_{\mathrm{I}}^{(n)} + \gamma_{\mathrm{I}}^{(n)} \beta_{\mathrm{R}}^{(1)} / \gamma_{\mathrm{R}}^{(1)}) + (\gamma_{\mathrm{I}}^{(n)}/\gamma_{\mathrm{R}}^{(1)}) \ln(A_1) + \varphi_n^0, \tag{19}$$

where $y_n = A_n \mathrm{e}^{\mathrm{j}\varphi_n}$, $y_{n+1} = A_n \mathrm{e}^{-\mathrm{j}\varphi_n}$ with $n = 3, 5, \ldots, N_c - 1$ where N_c is the number of the complex eigenvalues, A_n^0 and φ_n^0 are constants depending on the initial

[†] Real stable eigenvalues (eigenvectors) could be also considered in the present analysis [13]. The "slave modes" corresponding to zero-imaginary part eigenvalues should be given by

$$y_m(t) = y_m^0 \left(\frac{A_1}{A_1^0} \right)^{\gamma_R^{(m)}/\gamma_R^{(1)}} \mathrm{e}^{t(-\beta_R^{(m)} + \beta_R^{(1)} \gamma_R^{(m)}/\gamma_R^{(1)})}, \tag{47}$$

where the constants y_m^0 depend on the initial condition.

conditions and

$$\beta^{(n)} := \beta_R^{(n)} + \mathrm{j}\beta_I^{(n)} = -\lambda_n \mp \varepsilon\alpha_{nn} = -\lambda_n \mp \varepsilon \mathbf{v}^{(n)^{\mathrm{T}}} \mathbf{A}_1 \mathbf{u}^{(n)}, \tag{20}$$

$$\begin{aligned}\gamma^{(n)} := \gamma_R^{(n)} + \mathrm{j}\gamma_I^{(n)} &= -\varepsilon(\gamma_{nn12} + \gamma_{nn21} + \gamma_{n1n2} + \gamma_{n2n1} + \gamma_{n12n} + \gamma_{n21n}) \\ &= -\varepsilon \mathbf{v}^{(n)^{\mathrm{T}}} \Bigg\{ \sum_{p,q,r=1}^{N_s} c_{npqr} (u_p^{(n)} u_q^{(1)} u_r^{(2)} + u_p^{(n)} u_q^{(2)} u_r^{(1)} + u_p^{(1)} u_q^{(n)} u_r^{(2)} \\ &\quad + u_p^{(2)} u_q^{(n)} u_r^{(1)} + u_p^{(1)} u_q^{(2)} u_r^{(n)} + u_p^{(2)} u_q^{(1)} u_r^{(n)}) \Bigg\}, \quad n = 3, 5, \ldots . \end{aligned} \tag{21}$$

Thus, upon considering equations (5), (9), (13)–(15), (18) and (19), the response to initial conditions is

$$\begin{aligned}\mathbf{z} = \sqrt{\varepsilon} \Bigg(\mathbf{u}^{(1)} A_1 \mathrm{e}^{\mathrm{j}\varphi_1} + \mathbf{u}^{(2)} A_1 \mathrm{e}^{-\mathrm{j}\varphi_1} + \sum_{n=3}^{N_c} \mathbf{u}^{(n)} A_n \mathrm{e}^{\mathrm{j}\varphi_n} + \sum_{m=N_c+1}^{N_s} \mathbf{u}^{(m)} y_m \Bigg) \\ + \varepsilon\sqrt{\varepsilon} \mathbf{U} \Bigg\{ \sum_{s=1}^{N_s} \frac{\alpha_{js}^{\mathrm{aus}}}{\lambda_s - \lambda_j} y_s + \sum_{p,q,r=1}^{N_s} \frac{\gamma_{jpqr}^{\mathrm{aus}}}{\lambda_p + \lambda_q + \lambda_r - \lambda_j} y_p y_q y_r \Bigg\}. \end{aligned} \tag{22}$$

where $\alpha_{js}^{\mathrm{aus}} := \alpha_{js} - \alpha_{js}^{\mathrm{ess}}$ and $\gamma_{jpqr}^{\mathrm{aus}} := \gamma_{jpqr} - \gamma_{jpqr}^{\mathrm{ess}}$. Note that the contribution of the real (stable) eigenvalues has been also included (see reference [13]; for a higher order analysis considering only the critical mode of vibration but using higher order terms in equation (9), see reference [14]). Note also that the limit-cycle solution may be stable if (see reference [15]), although the linear part of the system is unstable, $\beta_R^{(1)} < 0$ (i.e. $\mu > \mu_0$), the non-linear part of the system is stable, $\gamma_R^{(1)} > 0$: i.e., if $\beta_R^{(1)} < 0$ and $\gamma_R^{(1)} > 0$ are both satisfied, a stable limit cycle may be observed in the post-critical response of the system. This case is interesting in an aeroelastic point of view because it represents a benign (non-linear) *flutter*, i.e., a stable limit cycle oscillation.

2.2. CONTINUOUS WAVELET TRANSFORM

The Fourier transform is a linear expansion of the signal into sinusoidal waveforms which have infinite length in time and that are extremely localized in frequency: this causes, in the frequency domain, the total loss of the time–information; correspondingly, the Fourier transform is not able to localize in the time–domain the instantaneous spectral features of the signal, i.e., it is not useful when it is necessary to analyze signals whose spectral characteristics are strongly time dependent. An improvement of the Fourier transform is given by the Fourier windowed transform (FWT; see reference [16] for theory and numerical applications): when using this transform, the signal is first enveloped with a time–window of given length and then Fourier-transformed. The FWT retains the time–information but has strong time–frequency resolution limitations: as

a matter of fact, if shorter windows are chosen, then one will have a higher time resolution but a coarser frequency resolution; on the other hand, if longer windows are chosen, then one will have a higher frequency resolution but a coarser time resolution. A superimposition of the windows can only partially bypass the resolution limitations.

In order to overcome these limitations [16, 17] in the last decade a new method, based on wavelets, has been developed. The wavelets are particular waveforms that, correlated to the signal, are able to show and identify its features with arbitrary frequency resolution at low frequencies and arbitrary time resolution at high frequencies [19]. Indeed, the only limitation to time–frequency resolution for this method is given by the uncertainty principle [18].

The continous wavelet transform $T^{wav}x$ of the signal $x(t)$ is defined as [19]

$$(T^{wav}x)(a, \tau) := \frac{1}{\sqrt{a}} \int_{-\infty}^{+\infty} x(t)\psi\left(\frac{t-\tau}{a}\right) \mathrm{d}t, \tag{23}$$

where a is the so-called *scaling parameter*, τ is the *localization parameter* and $\psi(t)$ is called *mother wavelet*. The previous transform has been performed for all the applications presented in this paper by using the *MATLAB Wavelet Toolbox* [17]. The set of wavelets $\psi^{a,\tau}$ is obtained by stretching or compressing the mother wavelet by the scaling parameter and localizing it by the parameter τ. Then, one has

$$\psi^{a,\tau}(t) = \frac{1}{\sqrt{a}}\psi\left(\frac{t-\tau}{a}\right). \tag{24}$$

The mother wavelet used in the present paper is the Morlet Wavelet [19] defined by

$$\psi(t) = \mathrm{e}^{-(t^2/2)}\mathrm{e}^{\mathrm{j}\omega_0 t}. \tag{25}$$

Specifically, in order to obtain real CWT functions one considers only the real part of the Morlet mother wavelet, with Fourier Transform given by (note that as ψ is real and the signals considered are also real; then, the CWT function given by equation (23) is real too)

$$\hat{\psi}(\omega) = \sqrt{\pi/2}\,(\mathrm{e}^{-(1/2)(\omega-\omega_0)^2} + \mathrm{e}^{-(1/2)(\omega+\omega_0)^2}), \tag{26}$$

where the symbol $\hat{}$ denotes the Fourier transform. This mother wavelet was chosen because it generates wavelets $\psi^{a,\tau}$ having sinusoidal waveforms with Gaussian envelope in the time–domain and Gaussian shape in the frequency–domain; therefore, these wavelets are similar, from a functional point of view, to vibration signals (and then, suitable to be correlated with these kind of signals) and in the meanwhile they are localized in time [see the Gaussian time function in equation (25)) and frequency (see equation (26)].

In Figure 1 the real and the imaginary parts of two Morlet Wavelets (with $\omega_0 = 2\pi$ rad/s) obtained for two different values of the scaling parameter are

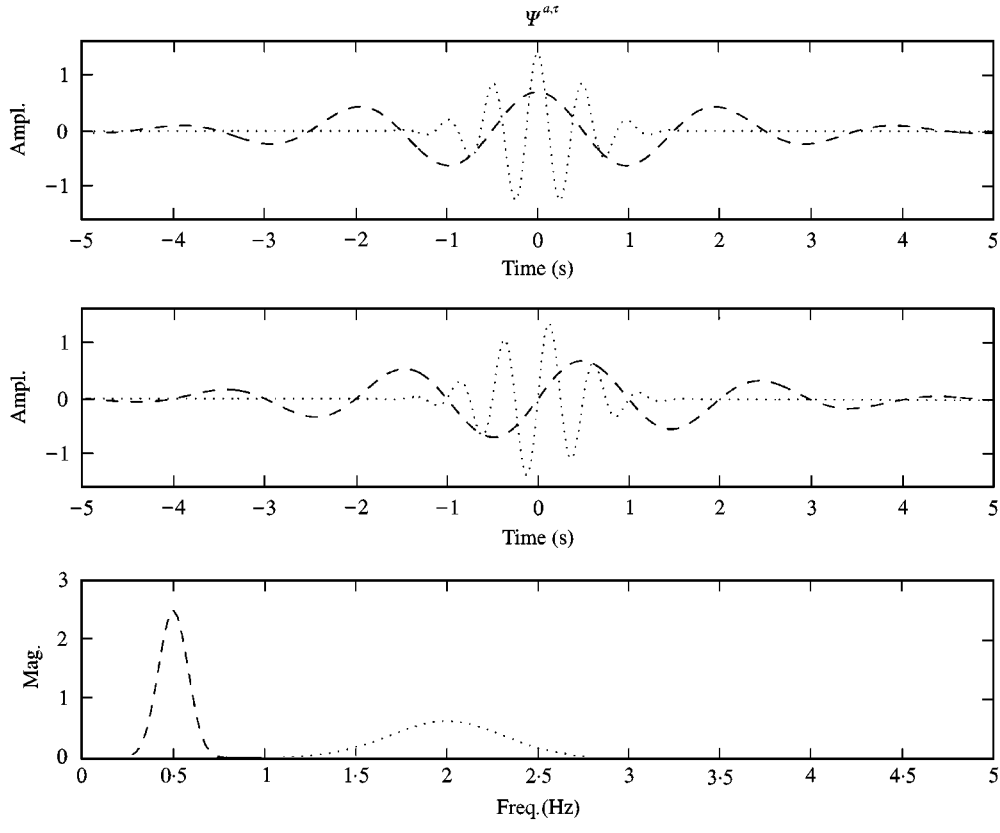

Figure 1. Real part, imaginary part, and Fourier transform of the real part of two Morlet wavelets (for · · · · · $a = 0{\cdot}5$ and − − − $a = 2$).

presented ($a = 0{\cdot}5$ and 2); furthermore, in the bottom figure the magnitude of the Fourier transform of their real part is also shown.

The continuous wavelet transform (CWT) of a signal may be represented in a time-scale plane, but on a time–frequency plane as well. As a matter of fact, the relation between frequency f and scale a is

$$a = \omega_0/2\pi f = \omega_0/\omega, \tag{27}$$

where ω is the angular frequency corresponding to the scale a. The previous equation allows one to map the time-scale plane in a time–frequency plane.

Substituting equation (25) in equation (23), we obtain:

$$(T^{wav}x)(a, \tau) = -\frac{1}{\sqrt{a}} \int_{-\infty}^{+\infty} \left[x(\tau - t)\, \mathrm{e}^{-1/2(t/a)^2} \right] \mathrm{e}^{-\mathrm{j}\omega t}\, \mathrm{d}t, \tag{28}$$

which shows the peculiarity of the CWT versus FWT: indeed, it is apparent that a CWT with Morlet Wavelet consists in Fourier transforming the signal enveloped

with Gaussian windows whose time length is not constant but depends on the frequency (i.e., on the scale parameter a). Specifically, the time length of the windows is small for high frequencies ω (small values of a) and large for low frequencies ω (large values of a).

It is necessary to find a formula able to reconstruct the time signal by its CWT because an inverse CWT may not exist for certain wavelet type [19]. The reconstruction formula could allow one to filter the signal in the time–frequency domain (directly filtering the CWT of the signal) and then to reconstruct the filtered signal in the time–domain. This reconstruction formula could also be used to find the frequency response functions (FRF) of a linear system, or to identify the linear part of non-linear systems. This can be carried out in a least-squares sense because the wavelets set given by equation (24) is not a set of orthogonal functions. In order to obtain that, one applies the Fourier transform to equation (23) from the domain τ to the domain $\bar{\omega}$ obtaining

$$\hat{T}^{wav}x(a, \bar{\omega}) = \sqrt{a}\hat{\psi}(a\bar{\omega})\hat{x}(\bar{\omega}), \tag{29}$$

where $\hat{x}(\bar{\omega})$ is the Fourier transform (from the time–domain) of the signal and $\hat{T}^{wav}x(a, \bar{\omega})$ is the Fourier transform of the CWT of the signal performed in the domain of the localization parameter τ. Thus, as $\hat{T}^{wav}x(a, \bar{\omega})$ and $\hat{\psi}$ are known functions, one can obtain (in a least-squares sense) $\hat{x}(\bar{\omega})$; then, applying the inverse of the Fourier transform (from the domain $\bar{\omega}$ to the domain t), one can find the reconstructed signal $x(t)$. Indeed, from a numerical point of view, equation (29) may be written for several values of the scaling parameter a, and the system of equations could then be solved in a least-squares sense,

$$\hat{x}(\bar{\omega}) = \frac{\begin{bmatrix} \hat{\psi}_{a_1}(\bar{\omega}) \\ \hat{\psi}_{a_2}(\bar{\omega}) \\ \vdots \\ \hat{\psi}_{a_M}(\bar{\omega}) \end{bmatrix}^{\mathrm{T}} \begin{bmatrix} \hat{T}^{wav}x(a_1, \bar{\omega}) \\ \hat{T}^{wav}x(a_2, \bar{\omega}) \\ \vdots \\ \hat{T}^{wav}x(a_M, \bar{\omega}) \end{bmatrix}}{\begin{bmatrix} \hat{\psi}_{a_1}(\bar{\omega}) \\ \hat{\psi}_{a_2}(\bar{\omega}) \\ \vdots \\ \hat{\psi}_{a_M}(\bar{\omega}) \end{bmatrix}^{\mathrm{T}} \begin{bmatrix} \hat{\psi}_{a_1}(\bar{\omega}) \\ \hat{\psi}_{a_2}(\bar{\omega}) \\ \vdots \\ \hat{\psi}_{a_M}(\bar{\omega}) \end{bmatrix}}, \tag{30}$$

where $\hat{\psi}_{a_i} = \sqrt{a_i}\hat{\psi}(a_i\omega)$ $(\mathrm{i} = 1 \cdots M)$ and M is the number of sampled values of a.

In Figure 2 the output of a *SDOF* viscous damped system is shown. The system was excited by using a chirp, i.e., a typical signal with a time-varying spectrum. In the top figure the original output signal x(t) is presented. In the middle figure is the signal first transformed via CWT and then reconstructed by using the proposed method (equation (30)), whereas in the third figure is the signal reconstructed obtained by using the method proposed in reference [2]. In Figure 3 the same

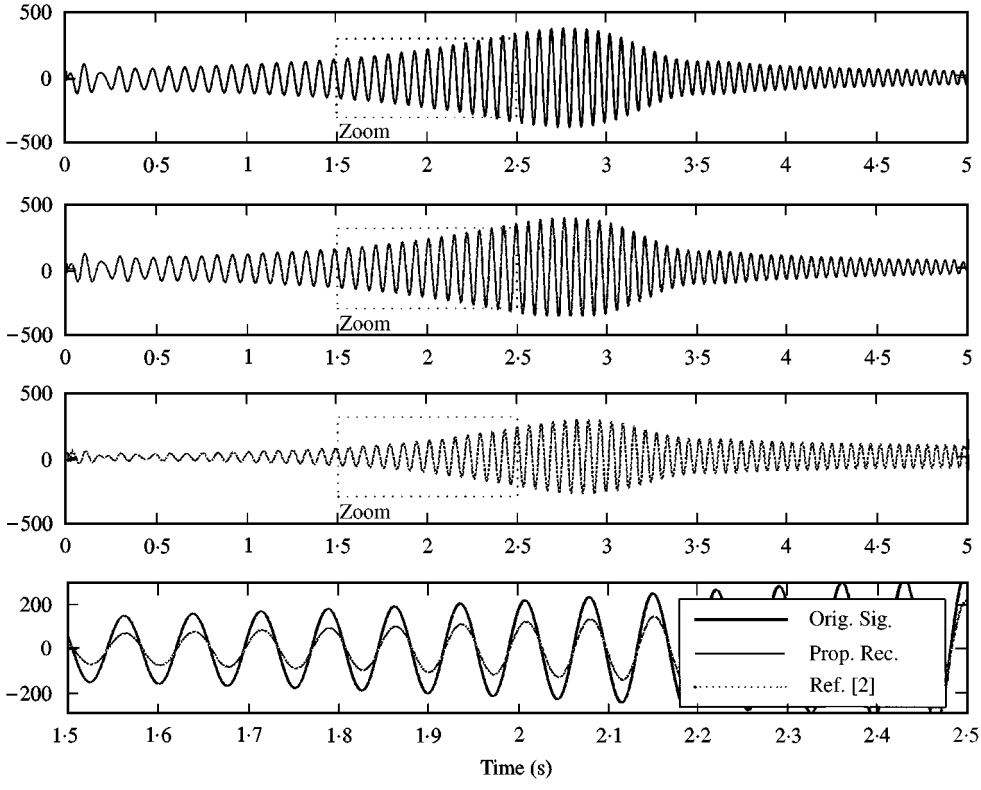

Figure 2. Signal reconstruction in the absence of noise: original signal (upper), proposed reconstruction (lower), reconstruction proposed in reference [2] (lower).

results are presented in the presence of noise: as one can see, in this case, the reconstructed signal is not punctually equal to the original signal. This is due to the fact that the system of equation (30) was solved in a least-squares sense: i.e., averaging the equations corresponding to different values of a.

2.3. RELATIONSHIP BETWEEN ANALYTICAL PREDICTIONS AND WAVELET ANALYSIS

In this section it is shown how the continuous wavelet transform (CWT) offers the possibility to identify the time-varying frequencies ω_i and the amplitudes A_i $(i = 1, \ldots, N_c)$ of a non-linear system in a Hopf bifurcation; as shown in section 2.1, these quantities can be analytically predicted by singular perturbation methods, once the response to initial conditions of a non-linear system is known.

From equation (22) one can see that the terms of order $\sqrt{\varepsilon}$ oscillate with the frequencies

$$\omega_1(t) := \frac{\partial \varphi_1}{\partial t} = -\beta_I^{(1)} + \gamma_I^{(1)} \frac{\beta_R^{(1)}/\gamma_R^{(1)}}{1 + k\mathrm{e}^{2\beta_R^{(1)}t}} \tag{31}$$

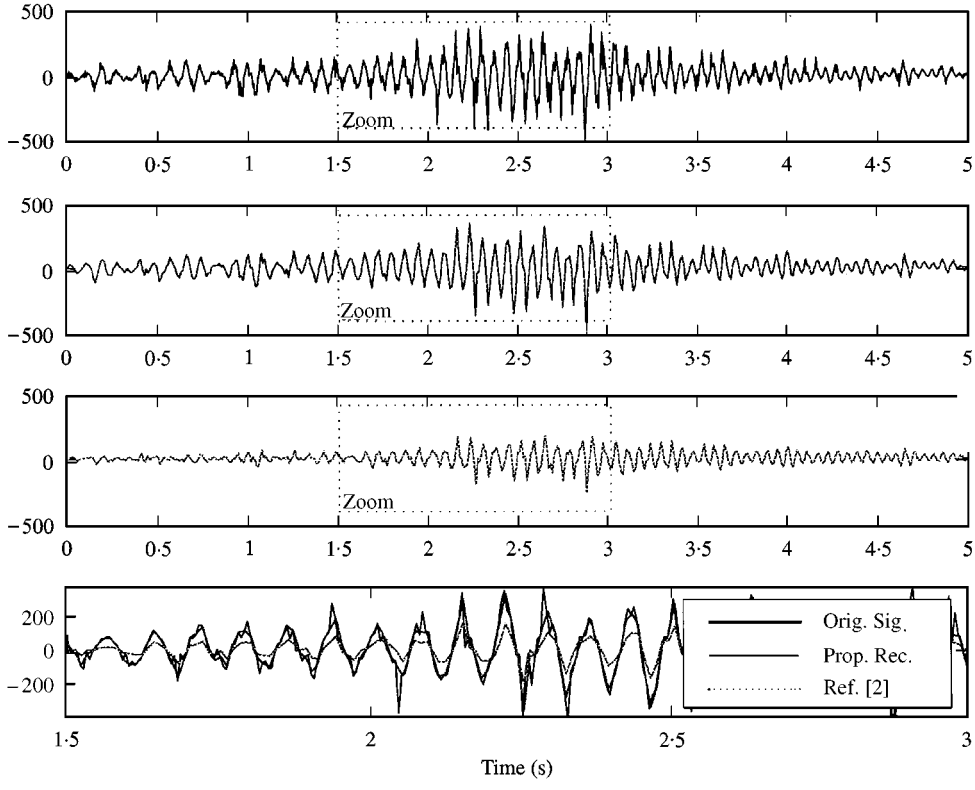

Figure 3. Signal reconstruction in the presence of noise: original signal (upper), proposed reconstruction (lower), reconstruction proposed in reference [2] (lower).

$$\omega_n(t) := \frac{\partial \varphi_n}{\partial t} = -\beta_I^{(n)} + \gamma_I^{(n)} \frac{\beta_R^{(1)}/\gamma_R^{(1)}}{1 + k e^{2\beta_R^{(1)} t}} \quad n = 3, \ldots, N_c, \tag{32}$$

$$\omega_m(t) := \frac{\partial \varphi_m}{\partial t} = 0 \quad m = N_c + 1, \ldots, N_s. \tag{33}$$

From equations (31) and (32) one can observe that the frequencies in the neighbourhood of the eigenvalues with non-zero imaginary part vary during the transient response. Thus, it is necessary to consider both the time- and the frequency-information (i.e., time-scale or time–frequency decompositions of the signal) if one wants to identify the non-linear nature of these systems.

In Figures 4 and 5 the function ω_1/ω_r is shown (where $\omega_r = \lim_{\tau \to +\infty} \omega_1(\tau)$) for different values of ε for post-critical tests, and in the two cases with $k < 0$ (Figure 4: initial conditions outside the limit cycle) and $k > 0$ (Figure 5: initial conditions inside the limit cycle). In order to describe the time evolution of these frequencies, a CWT function section at fixed $\tau = \bar{\tau}$ has been considered and its local maxima given by the condition (for continuous values of a)

$$\frac{\partial}{\partial a} |T^{wav} x(a, \bar{\tau})| = 0 \tag{34}$$

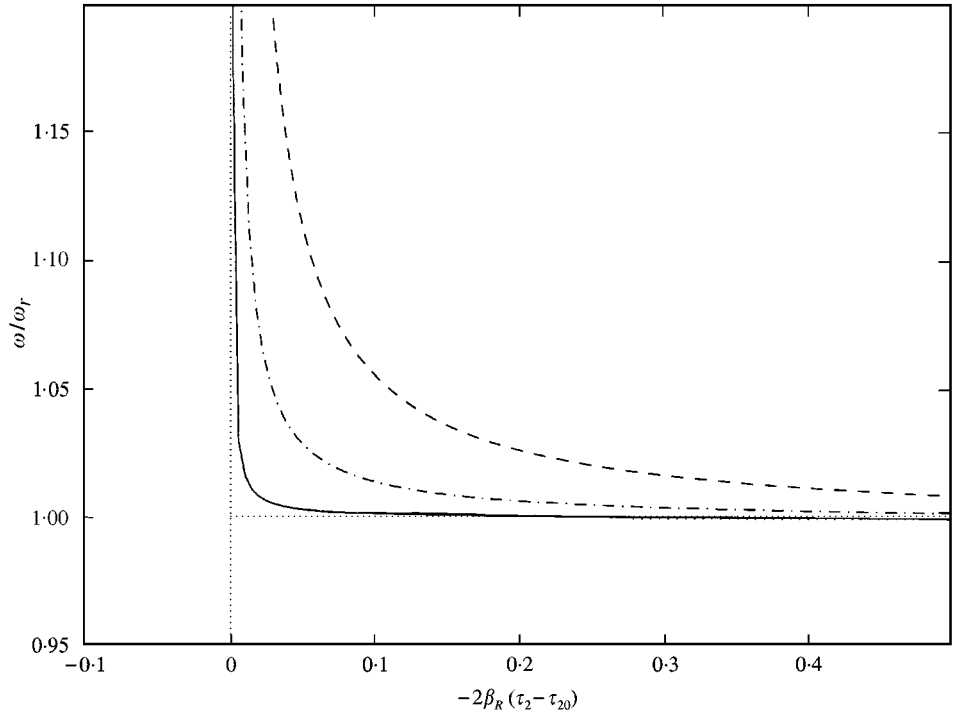

Figure 4. $\omega_1(\tau)$ (for $k < 0$ and $|\beta_R/\gamma_R| = 0{\cdot}5$); time evolution of ω_1 in the non-linear transient with the initial condition outside of the limit cycle. —— $\varepsilon = 0{\cdot}1$; –·–·– $\varepsilon = 0{\cdot}3$; – – – $\varepsilon = 0{\cdot}6$.

have been found. Repeating for different values of $\bar{\tau}$ one would be able to identify the functions $\omega_i(\tau)(\forall i = 1, 2, \ldots, N_c)$.† Once these frequency functions have been estimated it is possible to identify the functions $A_1, \ldots, A_n$ (see equations (14) and (18)) as shown in the remainder of this section: these functions are instantaneously proportional to the energy associated to each natural frequency and then are representative of the stability of each non-linear mode.

To find the relationship between $T^{wav}x(a, \tau)$ and the amplitudes A_i, one can first consider the response $x(t)$ to initial conditions of a *SDOF* viscous damped linear system. If ζ is the damping ratio and ω_n the natural undamped frequency, one has [4]

$$x(t) = \mathrm{e}^{-\zeta\omega_n t}\mathrm{e}^{\mathrm{j}(\omega_n\sqrt{1-\zeta^2}t+\varphi_0)} = A(t)\,\mathrm{e}^{\mathrm{j}(\bar{\omega}t+\varphi_0)}. \tag{35}$$

If $A(t)$ is slowly varying and, for simplicity, disregarding φ_0 one has [4]:

$$T^{wav}x(a, \tau) \simeq \frac{A(\tau)}{\sqrt{a}}\int_{-\infty}^{+\infty}\psi\left(\frac{t-\tau}{a}\right)\mathrm{e}^{-\mathrm{j}\bar{\omega}t}\,\mathrm{d}t \simeq \sqrt{a}\hat{\psi}(a\bar{\omega})A(\tau)\mathrm{e}^{-\mathrm{j}\bar{\omega}\tau}. \tag{36}$$

† It is worth pointing out that the identification of $\omega_i(\tau)$ is very important also because these functions depend on ε, i.e. on μ; thus, identifying $\omega_i(\tau)\forall i$ (or at least $\omega_1(\tau)$), in tests at different values of μ and knowing the structure of the analytical predictions (equations (31) and (32)) one could identify the critical value of the parameter (μ_0; see reference [9]).

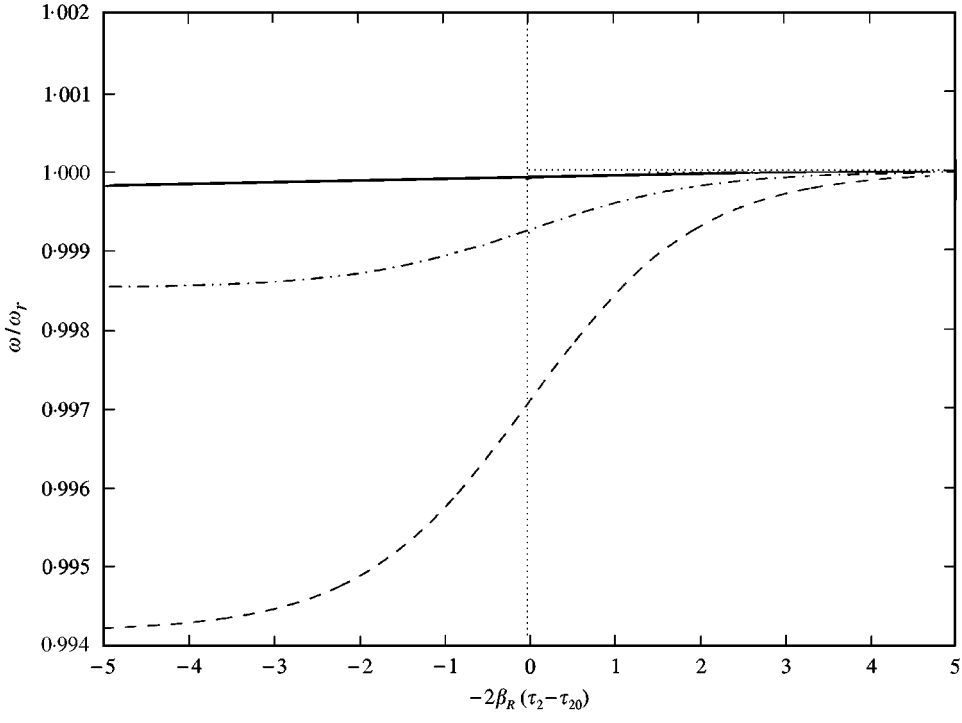

Figure 5. $\omega_1(\tau)$ (for $k > 0$ and $|\beta_R/\gamma_R| = 0{\cdot}5$); time evolution of ω_1 in the non-linear transient with initial condition inside of the limit cycle. —— $\varepsilon = 0{\cdot}1$; −·−·− $\varepsilon = 0{\cdot}3$; −−− $\varepsilon = 0{\cdot}6$.

Then, considering the envelope (here indicated with the symbol $|\ |$) of a cross section (a CWT section taken at fixed value of the scaling parameter a) of $T^{wav}x$ corresponding to the scale-parameter $\bar{a} = \omega_0/\bar{\omega}$ one has:

$$|T^{wav}x(\bar{a}, \tau)| \simeq \sqrt{\pi\omega_0/2\bar{\omega}}\, A(\tau). \tag{37}$$

As shown in reference [4], the previous equation holds for linear *MDOF* systems as well since the CWT is a linear transformation and the response to initial conditions of these systems is given by

$$x_i(t) = \sum_{k=1}^{N} B_{i,k}\, e^{-\zeta_k\omega_{n_k}t}\, e^{j(\omega_{n_k}\sqrt{1-\zeta_k^2}\,t+\varphi_k)} \equiv \sum_{k=1}^{N} A_{i,k}\, e^{j(\omega_{n_k}\sqrt{1-\zeta_k^2}\,t+\varphi_k)}. \tag{38}$$

For the sake of completeness, the hypothesis that the wavelets have, in the frequency domain, a compact support, should be also included [4]. In Figure 6 a numerical test on equation (37) is shown for the response of a 2 *DOF* coupled linear system: in the top figure the response (one of two *DOF*) is presented and in the last two figures the cross-sections of the CWT corresponding to the natural frequencies are shown, together with the theoretically predicted envelope functions (proportional to $A_{i,k} = B_{i,k}e^{-\zeta_k\omega_{n_k}t}$, see equation (37)). In Figure 7 the

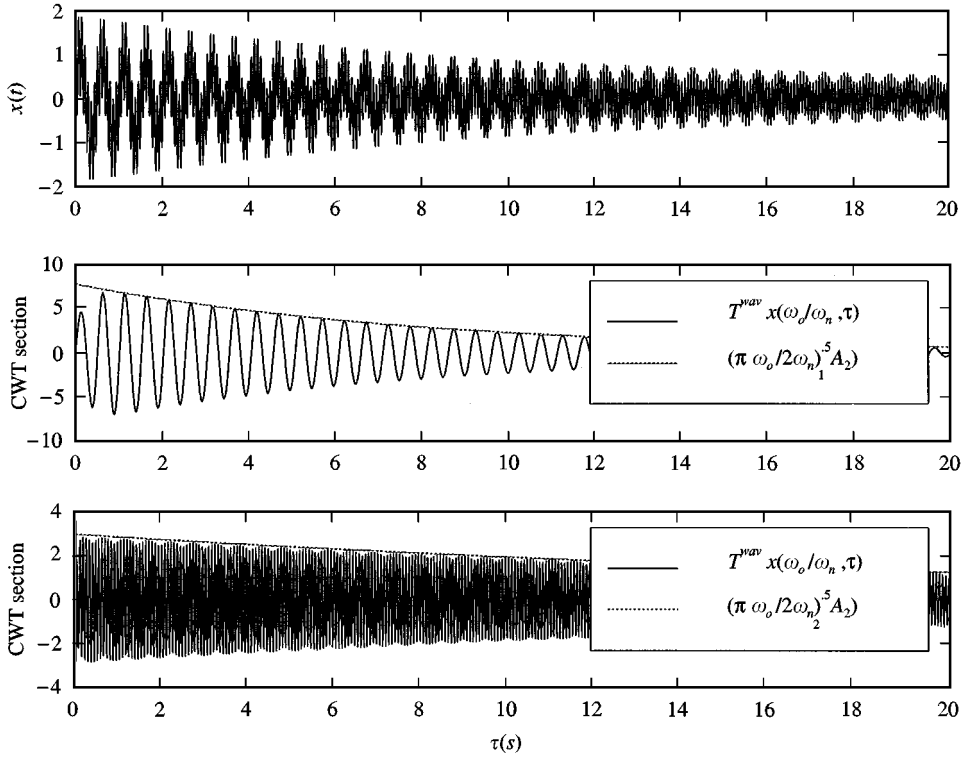

Figure 6. Proportionality between the cross-sections of CWT and predicted A_1, A_2 for a 2-*DOF* linear system ($f_{n_1} = 2{\cdot}0$ Hz, $\zeta_1 = 0{\cdot}01$, $f_{n_2} = 14{\cdot}0$ Hz, $\zeta_2 = 0{\cdot}0005$); time response (upper); cross-section of the CWT for $\omega = \omega_1$ (middle); cross-section of the CWT for $\omega = \omega_2$ (lower).

three-dimensional plot of the CWT coefficients shows that the development in time of the frequency content of the response for the two modes is clearly apparent.

Now considering an *MDOF* non-linear system in a Hopf bifurcation (equations (13)–(15), (18), (19) and (22)), one has that, if A_1, ω_1 are slowly varying functions, then

$$|T^{wav} y_1(a_1, \tau)| \simeq \sqrt{\pi\omega_0/2\omega_1}\, A_1(\tau), \tag{39}$$

where a_1 is the scale corresponding to ω_1. On the other hand, if A_n, ω_n and $\log A_1$ (see equations (19) and (32)) are slowly varying

$$|T^{wav} y_n(a_n, \tau)| \simeq \sqrt{\pi\omega_0/2\omega_n}\, A_n(\tau), \quad n = 3, \ldots, N_c. \tag{40}$$

Thus, the envelopes of the CWT logarithmic cross-sections, taken at the scales corresponding to the non-linear-characteristic frequencies, are proportional to the energy associated to that particular frequency and predicted by using the singular perturbation method. Equations (39) and (40) hold both for the pre- and post-critical behaviour.

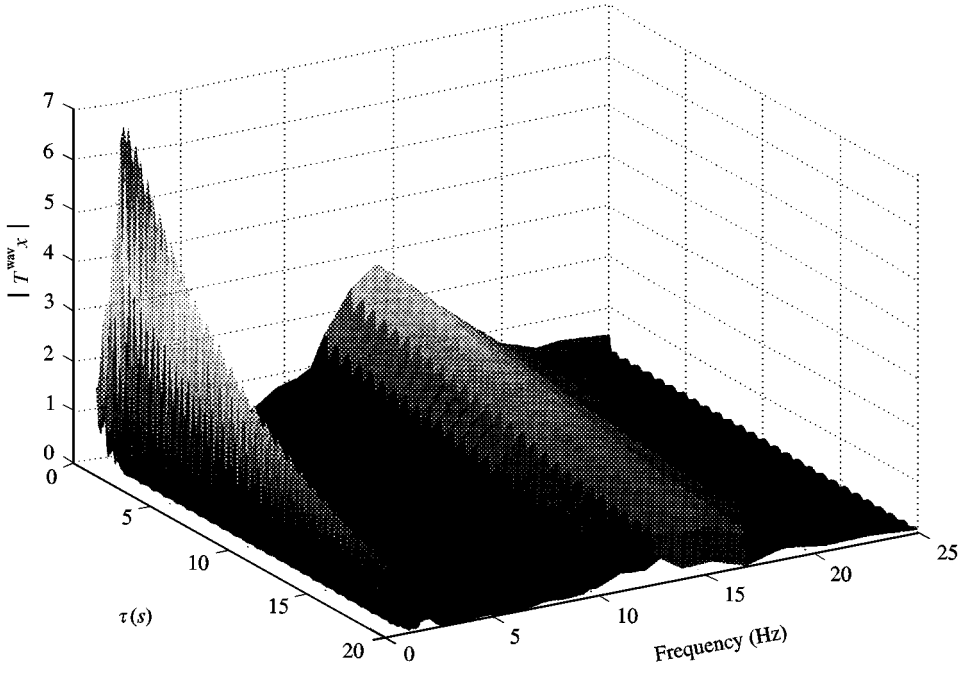

Figure 7. CWT of the response to initial conditions of a 2-*DOF* linear system.

Besides identifying the amplitude A_1, one may also identify the system's stability margins through pre-critical ($\mu < \mu_0$) simulations or tests. Taking the logarithm of equation (14) yields

$$\log A_1 = \frac{1}{2}\log\left|\frac{\beta_R^{(1)}}{\gamma_R^{(1)}}\right| - \frac{1}{2}\log(1 + k\mathrm{e}^{\beta_R^{(1)}t}). \tag{41}$$

In pre-critical conditions $\beta_R^{(1)} > 0$, then, if $k\mathrm{e}^{\beta_R^{(1)}t} \gg 1$, one obtains

$$\log|T^{wav}y_1(a_1, \tau)| \simeq \frac{1}{2}\log\frac{\pi\omega_0}{2\bar{\omega}} + \log A_1(t) \simeq K - \beta_R^{(1)}t. \tag{42}$$

Thus, the slope ϕ of the logarithm plot of the CWT cross-sections is analytically given by the coefficient $\beta_R^{(1)}$ and then is proportional to ε (from equation (16)). By identifying ϕ through several tests at different pre-critical values of μ, the CWT allows one to identify the system stability margin μ_0.

3. APPLICATIONS

In this Section two applications of the theory presented previously will be shown: first, for the sake of clarity, a very simple application to an oscillatory system will be presented; then a more complex application to an aerolastic system will be shown.

3.1. A SIMPLE NON-LINEAR MODEL

Consider the non-linear coupled oscillators described by the equations

$$\ddot{x}_1 + \omega_1^2 x_1 + \dot{x}_1\left[-\mu + \left(x_1^2 + \frac{1}{\omega_1^2}\dot{x}_1^2\right)\right] = 0, \tag{43}$$

$$\ddot{x}_2 + \omega_2^2 x_2 + \dot{x}_2\left[2\zeta\omega_2 - c_1\left(x_1^2 + \frac{1}{\omega_1^2}\dot{x}_1^2\right)\right] + x_1^3 = 0. \tag{44}$$

The eigenvalues corresponding to the linear part of the system depend on the parameter μ (with $|\mu| \ll 1$):

$$\lambda_{1,2} = \frac{\mu}{2} \pm \mathrm{j}\omega_1\sqrt{1 - \frac{\mu^2}{4\omega_1^2}} \simeq \frac{\mu}{2} \pm \mathrm{j}\omega_1, \tag{45}$$

$$\lambda_{3,4} = -\zeta\omega_2 \pm \mathrm{j}\omega_2\sqrt{1-\zeta^2} \simeq -\zeta\omega_2 \pm \mathrm{j}\omega_2. \tag{46}$$

Note that for $\mu < 0$ all of the eigenvalues have negative real parts (ζ is a viscous damping ratio), while for $\mu > 0$ two eigenvalues become unstable (thus, for this system one has $\mu_0 = 0$; see section 1). In Figure 8 the response to initial conditions, for pre- and post-critical values of the parameter μ, is presented. The initial conditions were chosen in order to excite both the natural modes of vibration relative to the linear part of the system. Upon observing the x_1 time–history in post-critical conditions, the incoming of a limit cycle is apparent; in the bottom figures (Figure 8) a zoom on the response is presented in order to show how the response evaluated by integrating numerically (Runge–Kutta method) equations (43) and (44) is very close to the one predicted by the singular perturbation method (indicated by Lie in Figure 8); the very small differences are due to the higher order terms.

Next, the results relative to the evaluation of the non-linear envelope functions and dominant frequencies of the limit-cycle via CWT will be shown. In Figure 9, by evaluating the CWT of the response, considering its sections at $\tau = \bar{\tau} = 100\,\mathrm{s}$ and finally finding the local maxima, the frequencies ω_1, ω_2 were identified: $T^{wav}x_1(a, \bar{\tau})$ and $T^{wav}x_2(a, \bar{\tau})$ are shown in the two cases $\mu < \mu_0$ (pre-critical conditions) and $\mu > \mu_0$ (post-critical conditions). In the sections one sees the evident local maxima denoting the instantaneously dominant frequencies (equation (34)).

Once these frequencies have been identified, it is possible to study the CWT cross-sections, for $\omega = \omega_1$ and ω_2, and then identify the amplitudes A_i (see equations (39) and (40)).

In Figure 10 the cross-sections (corresponding to the dominant frequencies ω_1 and ω_2) of the wavelet transform of the responses are shown: in the same figure the envelopes theoretically predicted by the perturbation analysis (equations (14) and (18)) are also depicted. One can see that only for very small values of τ there is

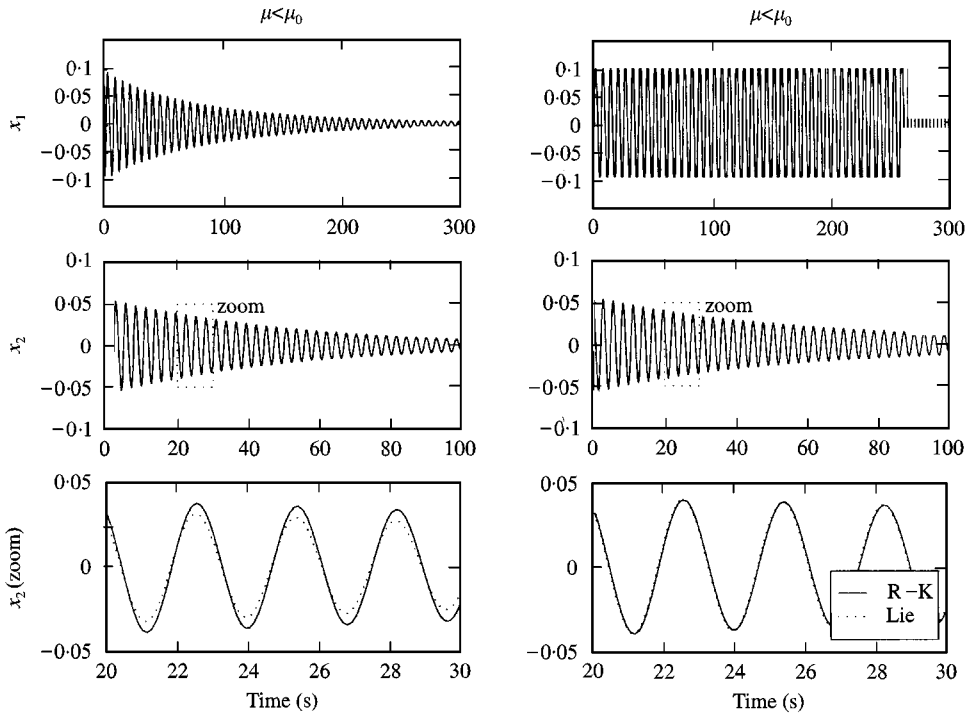

Figure 8. Response to initial conditions of the simple non-linear dynamic model ($\omega_1 = 1$ rad/s, $\omega_2 = 2{\cdot}234$ rad/s, $\delta = 0{\cdot}01$, $c_1 = 1$, $c_2 = c_3 = 0$) for pre-critical ($\mu = -0{\cdot}02$) and post-critical ($\mu = 0{\cdot}02$) conditions.

a relevant difference between the CWT cross-sections and their theoretically predicted envelopes. This is due to the truncation error that one has in evaluating the CWT coefficients for very small values of τ (for such values the wavelets $\psi^{a,\tau}$ are partially outside of the signal).

In Figure 11 the semi-logarithmic plot of the CWT cross section (for $\omega = \omega_1$) is shown for different values of $\mu < \mu_0$ (see equation (42)). Note that, the closer one is to the critical condition, the less is the slope ϕ of the CWT cross section (that directly represents the coefficient $\beta_R^{(1)}$). Evaluating the values of ϕ and interpolating them, one is able to estimate the value of the stability margin μ_0: in Figure 12 the linear interpolation is shown neglecting the presence of noise (thus for signal-to-noise ratio-SNR-equal to infinity). In Table 1 the μ_0 estimates ($\bar{\mu}_0$) are presented for different values of the SNR: from these results one can see that the method gives very good estimates for μ_0 even for very high SNR levels. This is probably due to several reasons: the first is that one is considering the amplitudes of the CWT cross-section (for $\omega =$ constant) and not the amplitudes of the response and this causes an operation of averaging in the time–domain, that reduces the effect of zero-average noise. Also, when one is considering only a cross-section of the CWT corresponding to the critical natural frequency, only the noise at this frequency can effectively affect the measurement. Furthermore, the least-squares procedure for the results obtained for different values of μ causes another average in the μ-domain.

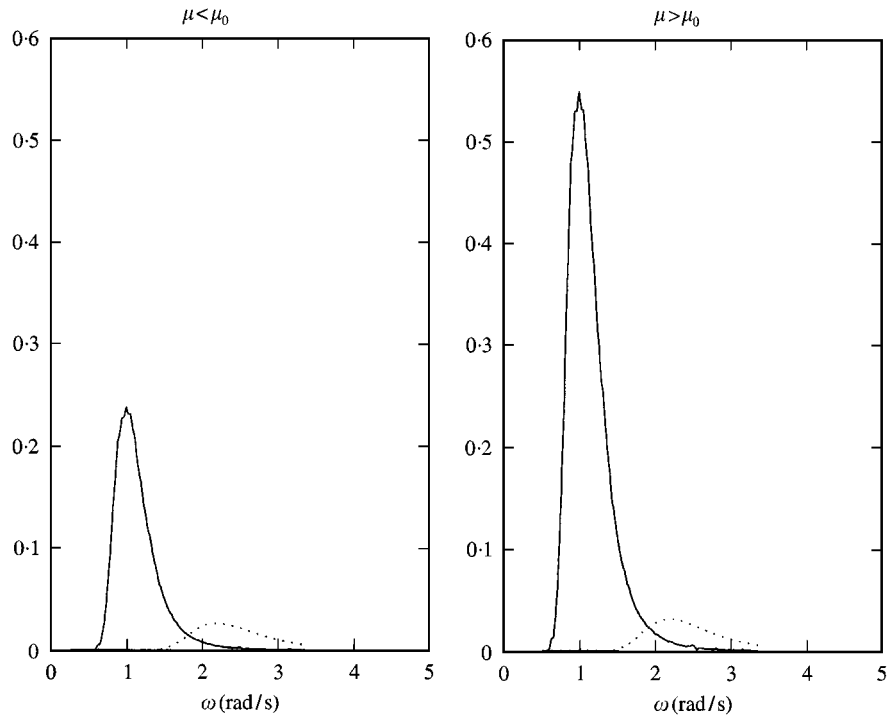

Figure 9. CWT sections for pre- and post-critical simulations. —— $T^{wav}x_1(a, \tau = 100\text{ s})$; · · · · $T^{wav}x_2(a, \tau = 100\text{ s})$.

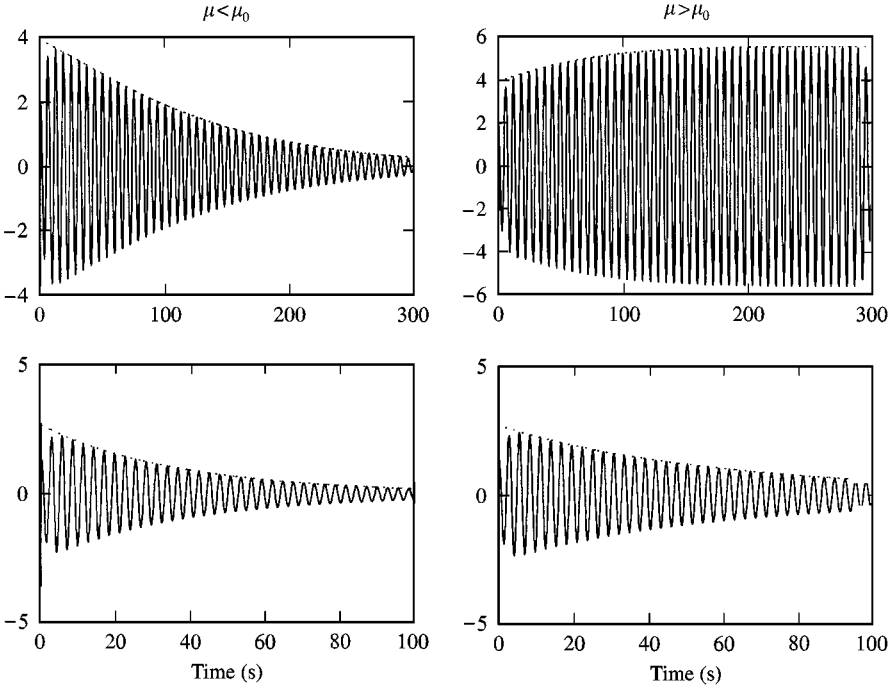

Figure 10. CWT cross-sections for x_1 (upper) x_2 (lower) and theoretically predicted envelopes (proportional to A_1, A_3). —— CWT c.s. · · · · Theor..

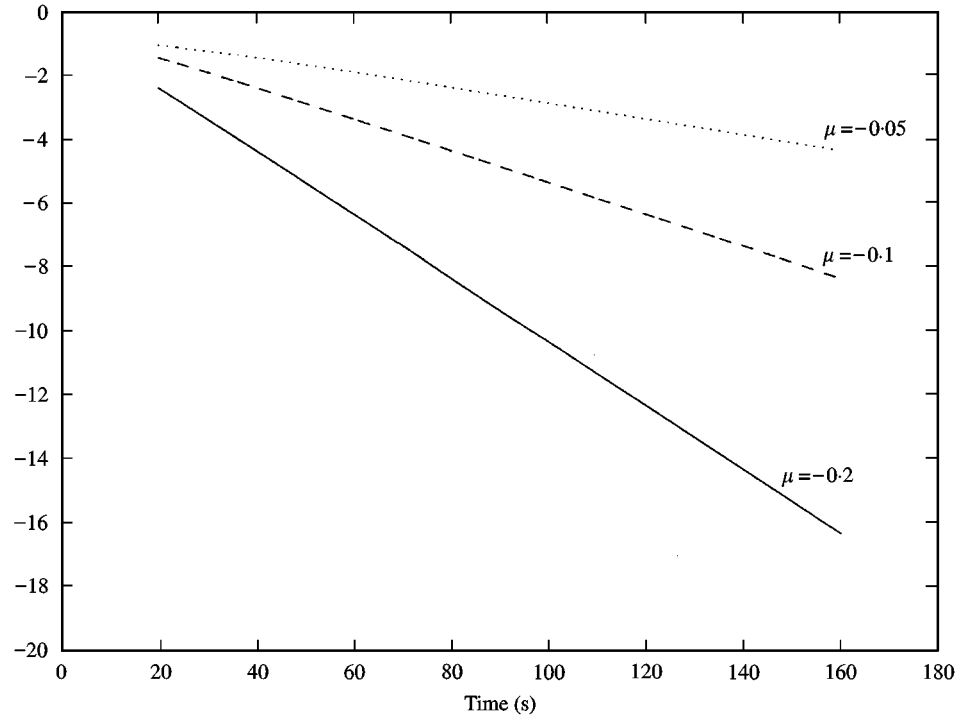

Figure 11. Semi-logarithmic plot of the CWT cross-sections for different values of the parameter μ.

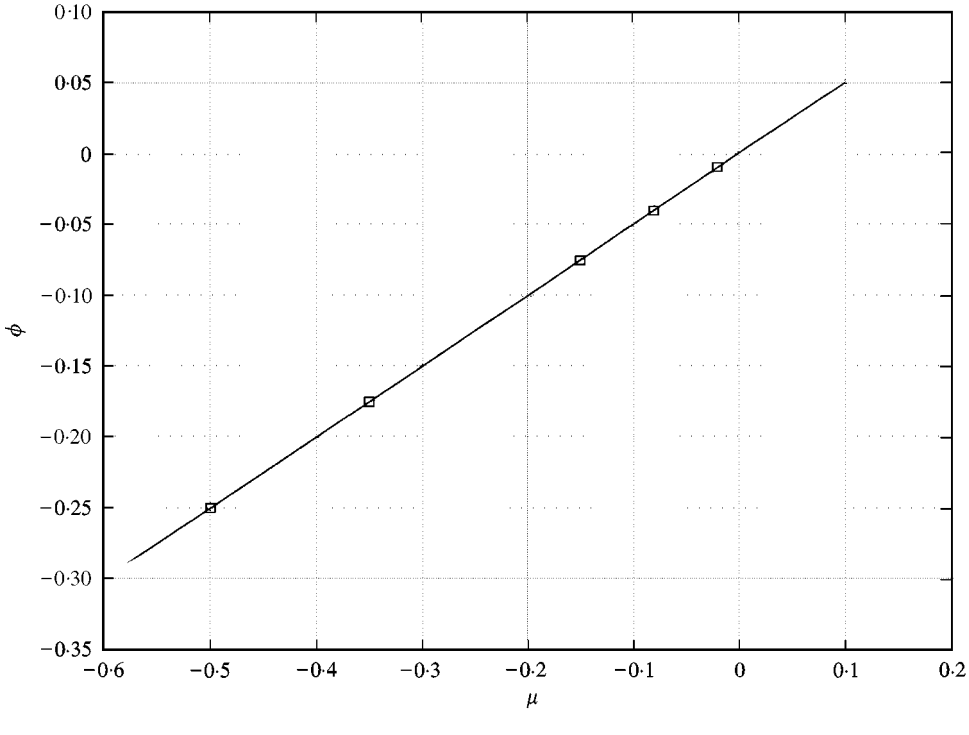

Figure 12. Identification of the system stability margin.

TABLE 1

Stability margin estimates

SNR	$\bar{\mu}_0$
$+\infty$	0
10 dB	− 0·0002
5 dB	− 0·008
2·5 dB	− 0·012

3.2. APPLICATION TO AN AEROELASTIC SYSTEM

The aeroelastic model considered is an airfoil in a supersonic flow with the unsteady-aerodynamic model given by the piston theory [20]. As shown in the Appendix A (see also reference [15] for similar applications), it is possible to find the state-space matrix **A** representing the linear part of the system and the vector **f** containing cubic non-linearities: these non-linearities are both structural (due to non-linear hardening and softening, translational and rotational springs) and aerodynamic.

Several numerical simulations were carried out for different combinations of the dimensionless parameters of the system, e.g., at different values of the Mach number M_∞. In Figure 13 the responses (plunge and pitch) are shown in pre-critical ($M_\infty = 2 < M_{\infty_F}$; $M_{\infty_F} = 2{\cdot}69$) and post-critical ($M_\infty = 3{\cdot}2 > M_{\infty_F}$) conditions. Since the non-linearities are stabilizing ($\gamma_R^{(1)} > 0$), the system presents a stable limit cycle for $M_\infty > M_{\infty_F}$; as one can see from Figure 13, the time histories found by numerical integration are very close to the ones obtained by using equation (22).

By analyzing the CWT sections for $\tau =$ constant (as shown in the previous section) the limit-cycle frequencies were identified; as in this case $\gamma_I^{(1)} \neq 0$, $\gamma_I^{(n)} \neq 0$, the natural frequencies vary during the transient response. Identifying the local maxima of the CWT sections for several values of $\bar{\tau}$, the wavelet transform has allowed one to identify $\omega_1(\tau)$, $\omega_3(\tau)$ predicted by equations (31) and (32). In Figures 14 and 15 the limit-cycle frequencies—as analytically predicted by perturbation analysis—are compared to the ones identified by using the FWT and the CWT estimates. As one can see from the figures, the CWT allows a better identification of ω_1, ω_3 because of its higher time-frequency resolution. It has to be pointed out that the variation of ω_1, ω_3 during the transient phase is dependent on the chosen initial condition (through the coefficients k and φ_0; see equations (14) and (15)); then, if the initial conditions are not so relevant, it may become very difficult to identify these functions because of their very small relative variations.

On the other hand, if ω_1 and ω_3 have small relative variations during the transient response, it is still possible to identify the amplitudes A_1 and A_3 by using the CWT cross-sections for $\omega = \omega_1$ and ω_2 respectively; in Figure 16 the CWT cross-sections of the time-history of the pitch angle, corresponding to the dominant frequencies, are shown. It has been found that while the identification of the theoretically predicted A_1 is very good, it is very difficult to identify the amplitude

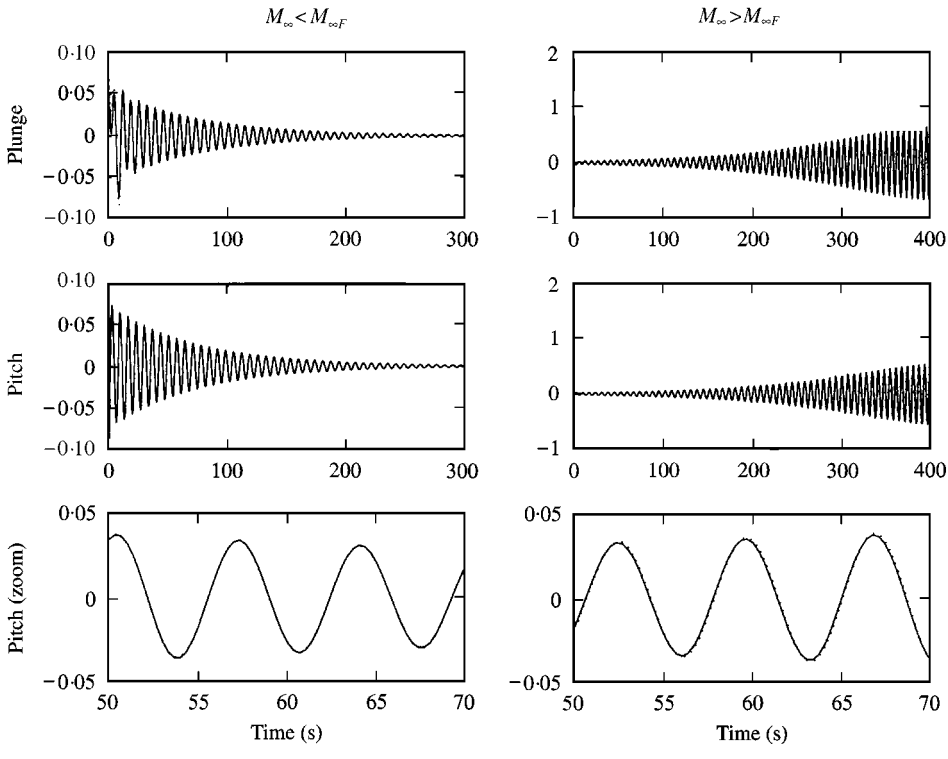

Figure 13. Response to initial conditions of an airfoil in a supersonic flow with cubic non-linearities ($M_\infty = 2$ and 3·2; $M_{\infty_F} = 2{\cdot}69$). —— R–K; · · · · Lie.

A_3: this happens because, besides considering the motivations exhibited in the previous application, the slave mode has a very high damping, so it dissipates energy much faster than the other mode, and the energy associated with it becomes quickly very small if compared with the energy associated to the critical mode. Then, the energy associated to the slave mode is considerable only at the very beginning of the time-history, where the truncation error in evaluating the CWT is still very high. In order to avoid this condition, one could choose the initial conditions in order to excite the slave mode significantly. All the modes performing this behaviour are highly damped, and then they are not so relevant for the identification of the system stability margin; in fact, in the following it is shown that it is necessary to identify the slope ϕ of the CWT semi-logarithmic cross sections. In Figure 17 the semi-logarithmic cross sections of the CWT envelopes of the pitch responses (corresponding to the frequency ω_1) are shown for different signal-to-noise ratios and different Mach numbers. As predicted by equation (42), ϕ linearly decreases as μ (i.e., M_∞) approaches μ_0 (M_{∞_F}); after identifying ϕ by using a least-squares straight line applied to the results obtained for different values of M_∞, the critical M_{∞_F} is robustly estimated. The results are also summarized in Table 2 and show a very low sensitivity to the noise level for the same reasons explained in the previous section; thus, the identification of the system stability margin through pre-critical tests with very low SNR (which is a very important and realistic

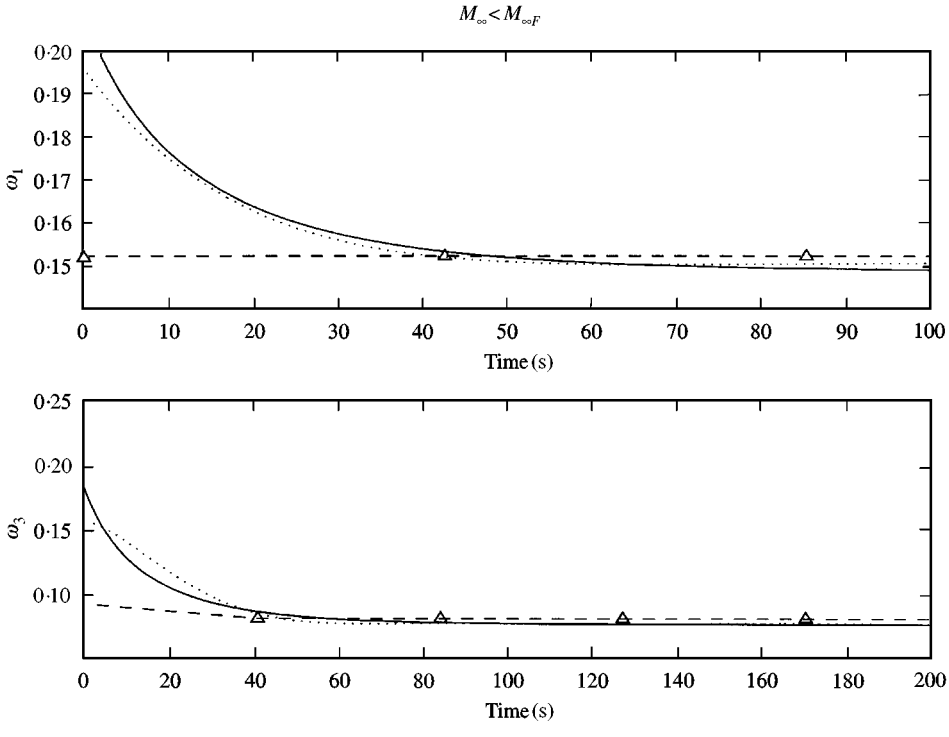

Figure 14. Identification of critical (top) and slave (bottom) characteristic frequencies for $M_\infty < M_{\infty_F}$. —— Theor.; · · · · CWT; –△– FWT.

experimental condition for flight tests) can be performed for such a non-linear system in the neighbourhood of a Hopf bifurcation.

4. CONCLUSIONS

In this paper a direct theoretical relationship between the analytical predictions of the responses of non-linear systems in the neighbourhood of a Hopf bifurcation (obtained by the singular perturbation analysis) and the results of a time-scale analysis applied on the time data via the continuous wavelet transform has been found and verified. This link has been established by exploiting the opportunity, given by wavelet analysis, to analyze and capture the features of transient responses (e.g., a time-varying spectral content). This relation has also allowed the identification of the system main features (e.g., non-linearity) by examining its response to initial conditions in the absence and also in the presence of noise. Specifically, it allows one to identify the characteristic frequencies (that are the natural frequencies in the case of free response of linear systems) which are not constant during the transient response of non-linear systems. Furthermore, it allows one to identify the stability of each mode of the linear part of the system, the incoming of a limit cycle, and the system stability margin through pre-critical tests. The proposed methods have been shown to have a very low noise sensitivity; thus

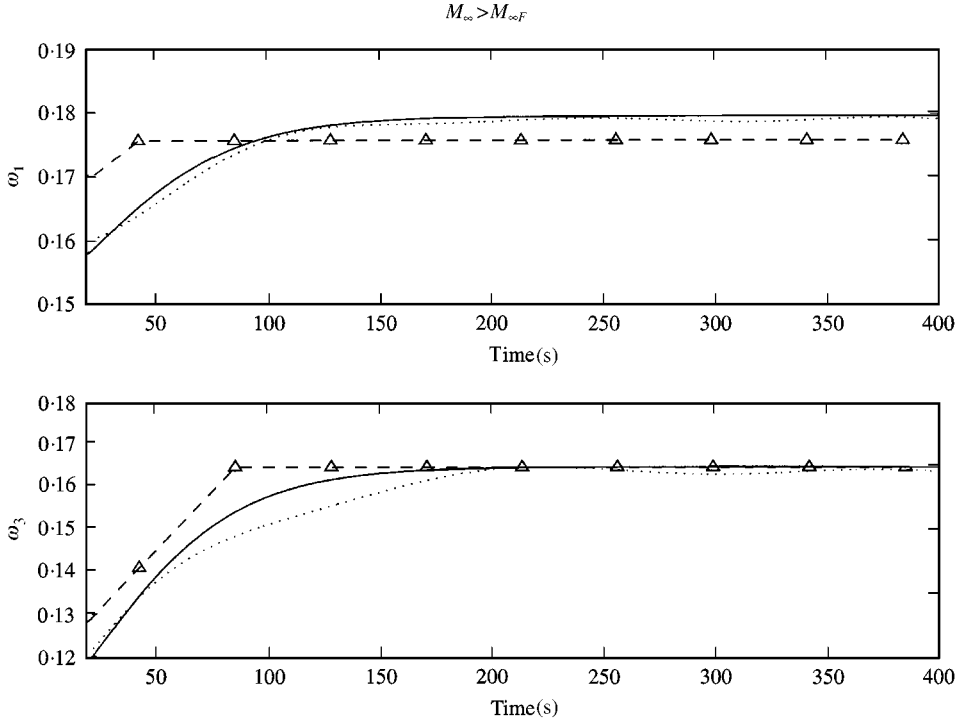

Figure 15. Identification of critical (top) and slave (bottom) characteristic frequencies for $M_\infty > M_{\infty_F}$. —— Theor.; · · · · CWT; –△– FWT.

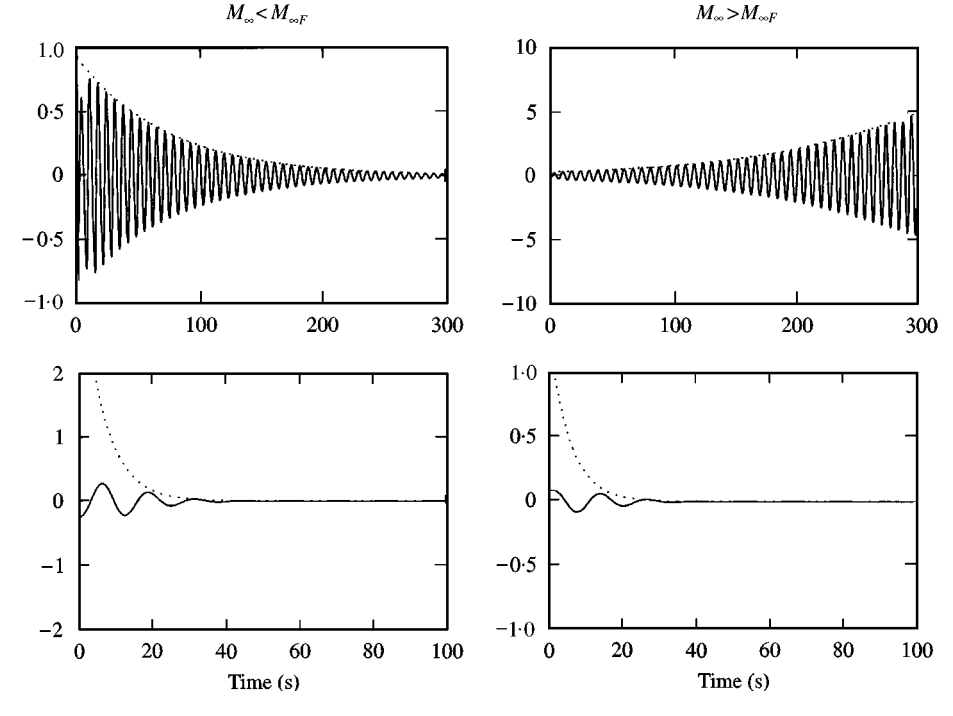

Figure 16. CWT cross sections and theoretically predicted (perturbation analysis) envelopes ($M_\infty = 2$ and 3·2; $M_{\infty F} = 2{\cdot}69$). —— CWT c.s.; · · · · Theor..

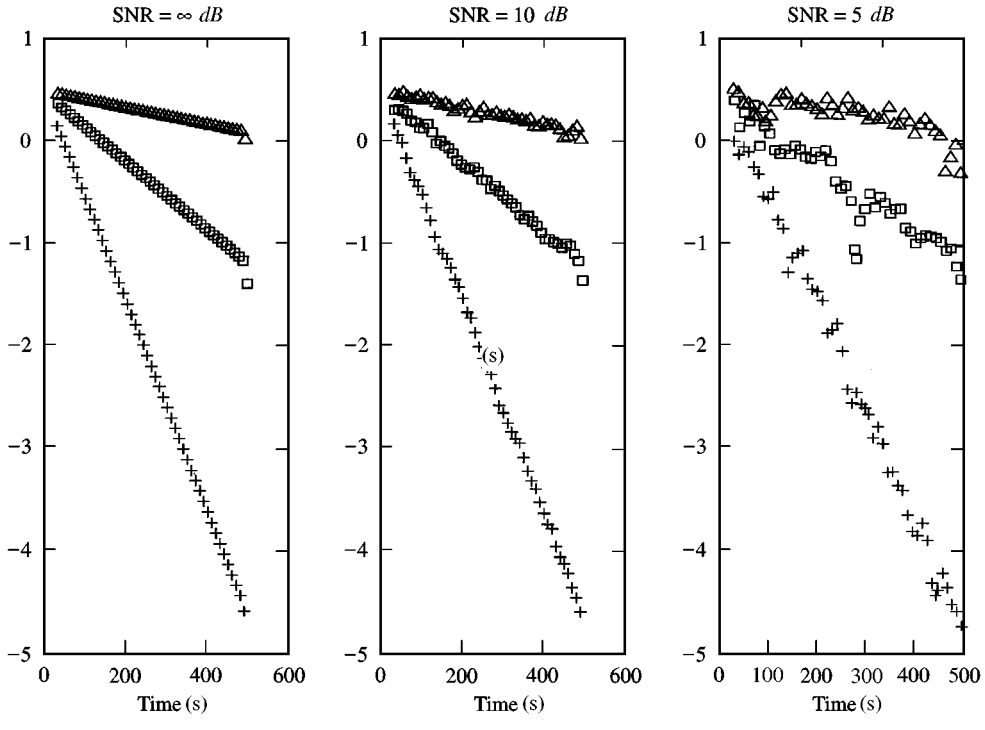

Figure 17. Semi-logarithmic plot of CWT cross sections for different values of the M_∞ and of the signal-to-noise ratio. $+ M_\infty = 1{\cdot}5$; $\square$ $M_\infty = 2{\cdot}3$; $M_\infty = 2{\cdot}5$.

TABLE 2

Stability margin estimates: ε is the error in percent on the flutter-boundary estimate

SNR	$\bar{M}_{\infty_F}$	ε (%)
$+\infty$	2·693	0·096
10 dB	2·688	− 0·107
5 dB	2·687	− 0·145
2·5 dB	2·685	− 0·219

they might be efficiently applied to time-histories obtained by real aeroelastic flight tests or by those of a general non-linear systems in the neighbourhood of a Hopf bifurcation.

ACKNOWLEDGMENTS

This work has been supported by the University of Rome I "*La Sapienza*," finanziamento progetti di ricerca afferenti la quota 60% (ricerche di Facoltà), grant 1996: "*Controllo Nonlineare della Stabilità di Sistemi Aeroelastici in Fase Pre- e Post-Critica.*"

REFERENCES

1. M. J. Brenner, R. C. Lind and D. F. Voracek 1997 *NASA Technical Memorandum* 4792. Overview of recent flight flutter testing research at NASA Dryden.
2. M. J. Brenner 1997 *NASA Technical Memorandum* 4793. Wavelet analyses of F/A-18 aeroelastic and aeroservoelastic flight test data.
3. R. Lind, M. Brenner and S. Haley 1997 *AIAA Atmosferic Flight Mechanics Conference, New Orleans, California.* Estimation of modal parameters using a wavelet-based approach.
4. W. J. Staszewski 1997 *Journal of Sound and Vibration* **203**, 283–305. Identification of damping in MDOF systems using time-scale decomposition.
5. L. Freudinger, R. Lind, and M. Brenner 1998 *16th IMAC, Santa Barbara, California.* Correlation filtering of modal dynamics using the Laplace wavelet.
6. M. Brenner 1998 *AIAA Structures, Structural Dynamics and Materials Conference Paper 98-1896, Long Beach, California.* Wavelet filtering to reduce conservatism in aeroservoelastic robust stability margin.
7. R. Lind, K. Snyder, and M. Brenner 1998 *AIAA Structures, Structural Dynamics and Materials Conference Paper 98-1808, Long Beach, California.* Investigating transient and limit cycle behaviours of a nonlinear structure by wavelet transforms.
8. A. H. Nayfeh 1993 *The Method of Normal Forms.* New York: Wiley.
9. A. Bettoli 1998 *Master thesis in Aerospace Engineering, University of Rome La Sapienza.* Analisi di segnali tramite trasformate "wavelets" per l'identificazione di sistemi aeroelastici.
10. F. Mastroddi and L. Morino 1996 *The Aeronautical Journal* **100**, 389–396. Limit-cycle taming by nonlinear control with application to flutter.
11. E. H. Dowell, L. N. Virgin, D. M. Tang and M. D. Conner 1997 *Proceedings of CEAS International Forum on Aeroelasticity and Structural Dynamics, Rome,* **I**, 79–91. Nonlinear dynamics of aeroelastic systems.
12. F. Mastroddi 1994 *Ph.D. thesis in Aerospace Engineering, University of Rome La Sapienza.* Aeroservoelasticità: problematiche non Lineari.
13. L. Morino F. Mastroddi and M. Cutroni 1995 *Nonlinear Dynamics* **7**, 403–428. Lie transformation method for dynamical systems having chaotic behaviour.
14. D. Dessi, L. Morino and F. Mastroddi 1997 *Proceedings of CEAS International Forum on Aeroelasticity and Structural Dynamics, Rome,* **I**, 79–91. A fifth-order no-reconstruction multiple-scale solution for Hopf-bifurcations.
15. L. Smith and L. Morino 1976 *AIAA Journal,* **14**, 333–341. Stability analysis of nonlinear differential autonomous systems with applications to flutter.
16. T. P. Krauss, L. Shure and J. N. Little 1992 *Signal Processing Toolbox for Use with MATLAB©*. Massachussets; The Math Work Inc.
17. M. Misiti, Y. Misiti, G. Oppenheim and J. M. Poggi 1996 *Wavelet Toolbox for Use with MATLAB©*. Massachussets; The Math Work Inc.
18. M. Vetterli and J. Kovacevic 1995 *Wavelets and Subband Coding.* New Jersey; Prentice-Hall.
19. I. Dauberchies 1992 *Ten Lectures on Wavelets.* Philadelphia: SIAM.
20. H. Ashley and G. Zartarian 1956 *Journal of Aeronautical Sciences* **23**, 1109–1118. Piston theory—a new aerodynamic tool for the aeroelastician.

APPENDIX A

In this appendix the equations governing the non-linear flutter of an airfoil in a supersonic flow will be presented (see also reference [15]). The motion $\mathbf{x}(\zeta, t)$ may be written as

$$\mathbf{x}(\zeta, t) = \mathbf{x}_0 + \mathbf{u}(\zeta, t), \tag{A1}$$

where ζ is the section chordwise co-ordinate, $\mathbf{x}_0$ is the equilibrium position and the displacement $\mathbf{u}(\zeta, t)$ is assumed to be a linear combination of the functions $\phi_r(\zeta)$:

$$\mathbf{u}(\zeta, t) = \sum_r u_r(t)\,\phi_r(\zeta). \tag{A2}$$

Upon considering for a rigid airfoil, as degrees of freedom, the vertical displacement ($u_1(t) = h(t)$) and the rigid rotation ($u_2(t) = \alpha(t)$), the corresponding assumed functions become: $\phi_1(\zeta) = \mathbf{k}$, $\phi_2(\zeta) = -(\zeta - \zeta_c)\mathbf{k}$; where $\mathbf{k}$ is the unit vector normal to the chordwise and spanwise directions and ζ_c is the abscissa of the centre of mass.

With m and J_c the mass and the moment of inertia (with respect to the centre of mass) of the airfoil, the Lagrange equations of motion become

$$m\ddot{h} + \partial\mathscr{E}/\partial h = e_h, \quad J_c\ddot{\alpha} + \partial\mathscr{E}/\partial\alpha = e_\alpha, \tag{A3, A4}$$

where $\mathscr{E}$ is the elastic energy and e_h, e_α are the generalized forces associated with the assumed modes (whose expression is $e_r = \oint_C \mathbf{t}\cdot\phi_r\,\mathrm{d}s$, $\mathbf{t}$ being the aerodynamic force per unit length).

For a non-linear elementary model and the elastic energy is expressed as

$$\mathscr{E} = \tfrac{1}{2}k_h(h + \Delta\alpha)^2 + \tfrac{1}{4}k'_h(h + \Delta\alpha)^4 + \tfrac{1}{2}k_\alpha\alpha^2 + \tfrac{1}{4}k'_\alpha\alpha^4, \tag{A5}$$

where $\Delta = \zeta_c - \zeta_e$ (ζ_e is the elastic center abscissa) and k_h, k'_h, k_α, and k'_α are elastic constants.

The non-linear piston theory is used [20] and then the pressure distribution is given by

$$p = p_\infty\left[1 + \frac{1}{2}\left(\frac{c_p}{c_v} - 1\right)\frac{w}{a_\infty}\right]^{2c_p/c_p - c_v}, \tag{A6}$$

where the downwash is given by

$$w = (1/n_z)\{[\dot{h} - (\zeta - \zeta_c)\cos\alpha\dot{\alpha}]n_z - U_\infty n_\zeta\} \tag{A7}$$

and U_∞, a_∞ are the velocity of the flow and the speed of sound; c_p, c_v the specific heats of the air and $n_\zeta = \mathbf{n}\cdot\mathbf{i}$, $n_z = \mathbf{n}\cdot\mathbf{k}$ where $\mathbf{i}$ is the chordwise unit vector.

Combining the preceeding equations, for a zero-thickness, uncambered airfoil, and neglecting the higher order terms, one has that the model is described by

$$\dot{\mathbf{x}} = \mathbf{A}_\mu\mathbf{x} + \mathbf{f}(\mathbf{x}, \mu), \tag{A8}$$

where the state-space variables are: $\mathbf{x}^{\mathrm{T}} = [\xi, \alpha, \dot{\xi}, \dot{\alpha}]$. Upon using the dimensionless parameters:

$$\xi = h/b,\ \tau = ta_\infty/b,\ M_\infty = U_\infty/a_\infty,\ \Omega_\xi^2 = k_h b^2/ma_\infty^2,\ \Omega_\alpha^2 = k_\alpha b^2/J_c a_\infty^2,$$

$$\delta = \Delta/b,\ \nu = J_c/mb^2,\ \eta = m/4\rho_\infty b^2,\ \sigma = 1/\eta,\ \alpha = 4U_\infty\rho_\infty b^2/ma_\infty, \tag{A9}$$

the coefficients of the system are

$$\mathbf{A} = \begin{bmatrix} 0 & 0 & 1 & 0 \\ 0 & 0 & 0 & 1 \\ -\Omega_\xi^2 & -\Omega_\xi^2\delta & -\sigma S_0 & \sigma S_1 \\ -\Omega_\xi^2\delta/v & -(\Omega_\xi^2\delta^2 + v\Omega_\alpha^2)/v & \sigma S_1/v & -\sigma S_2/v \end{bmatrix} + \alpha \begin{bmatrix} 0 & 0 & 0 & 0 \\ 0 & 0 & 0 & 0 \\ 0 & S_0 & 0 & 0 \\ 0 & -S_0/v & 0 & 0 \end{bmatrix}, \tag{A10}$$

$$\mathbf{f} = \begin{bmatrix} 0 \\ 0 \\ f_\xi \\ f_\alpha/v \end{bmatrix} + \begin{bmatrix} 0 \\ 0 \\ g_\xi \\ g_\alpha/v \end{bmatrix}, \tag{A11}$$

where: $S_n = (1/2b)\int_{-b}^{b}[(\zeta - \zeta_c/b)]^n \,\mathrm{d}\zeta$ $(n = 0 \ldots 4)$, and

$$f_\xi = \tfrac{1}{6} K_{12}\alpha^3 - \hat{k}_\xi(\xi + \delta\alpha)^3, \tag{A12}$$

$$f_\alpha = \tfrac{1}{2} K_{12}\xi\alpha^2 + \tfrac{2}{3}\Omega_\xi^2\delta^2\alpha^3 - \delta\hat{k}_\xi(\xi + \delta\alpha)^3 - v\hat{k}_\alpha\alpha^3, \tag{A13}$$

$$g_\xi = \sigma(-\tfrac{1}{6} S_0 M_\infty\alpha^3 + \tfrac{1}{2} S_0\alpha^2\dot{\xi} - S_1\alpha^2\dot{\alpha}) + \chi\sigma[S_0(M_\infty\alpha - \dot{\xi})^3 + 3S_1(M_\infty\alpha - \dot{\xi})^2\dot{\alpha} + 3S_2(M_\infty\alpha - \dot{\xi})\dot{\alpha}^2 + S_3\dot{\alpha}^3], \tag{A14}$$

$$g_\alpha = \sigma(-\tfrac{1}{3} S_1 M_\infty\alpha^3 + \tfrac{1}{2} S_2\alpha^2\dot{\alpha}) - \chi\sigma[S_1(M_\infty\alpha - \dot{\xi})^3 + 3S_2(M_\infty\alpha - \xi)^2\dot{\alpha} + 3S_3(M_\infty\alpha - \dot{\xi})\dot{\alpha}^2 + S_4\dot{\alpha}^3], \tag{A15}$$

and $\hat{k}_\xi = (k_h' b^4/ma_\infty^2)$, $\hat{k}_\alpha = (k_\alpha' b^2/J_c a_\infty^2)$ and $\chi = (1 + c_p/c_v)/12$.